Electronic Supplementary Material (ESI) for Energy & Environmental Science

Electronic Supplementary Information for

A tubular polypyrrole based air electrode with improved O_2 diffusivity for Li-O_2 batteries

Yanming Cui, Zhaoyin Wen*, Xiao Liang, Yan Lu, Jun Jin, Meifen Wu and Xiangwei Wu

CAS Key Laboratory of Materials for Energy Conversion,
Shanghai Institute of Ceramics, Chinese Academy of Sciences,
Shanghai, China, 200050
Fax: +86-21-52413903; Tel: +86-21-52411704;
E-mail: zywen@mail.sic.ac.cn

1 Experimental

1.1. Preparation and characterization of tubular PPy (TPPy) and granular PPy (GPPy)

The tubular PPy was synthesized by a typical self-degraded template method. The synthesis process was described as follows: $FeCl_3$ (10.5 mmol) and Methyl Orange (1.05 mmol) were dissolved in 210 ml H_2O. Then 10.5 mmol pyrrole was added to it and stirred for 24 h at room temperature. The product obtained was washed with water and ethanol alternatively until the filtrate was colorless, and then dried under vacuum at 50 °C for 24 h. The granular GPPy was synthesized by a chemical oxidation method. The detailed synthetic process was the same as that of TPPy just in absence of Methyl Orange.

The structure of the as-prepared samples was characterized by Fourier Transform Infrared Spectroscopy (FTIR) (Tensor 27) in transmission with a KBr pellet. The morphology of the synthesized materials was observed on a field emission scanning electron microscope (FESEM JSM-6700F) and a transmission electron microscope (TEM JEM-2100F). The wetting angle of the electrolyte on different supports was measured on an EasyDrop (a contact angle measuring instrument, model EasyDrop DSA15B, KRÜSS, Germany) at room temperature in 1 atm of Ar. The N_2 sorption measurement was performed using Micromeritics Tristar 3000 at 77K, and specific surface area was calculated using the Brunauer–Emmett–Telley (BET).

1.2. Electrode preparation and Li-O_2 cell assemblage

The PPy nanotubes were used as supports for the air electrodes. The cathode was formed by casting a ball-milled slurry of the as-prepared TPPy with the electrolytic manganese dioxide (EMD) as a catalyst, and polyvinylidene fluoride (PVDF) as a binder (with a same weight ratio of 11:19:15 as in the report [1]) onto a stainless steel mesh as cathode current collector (both sides). So as to more clearly evaluate the improvement in oxygen diffusion by TPPy, the as-prepared composite electrodes were pressed to a disc with thickness of 1500 ± 20 μm. The electrochemical

cells used were based on a Swagelok design composed of a Li metal anode (14 mm in diameter, 0.5 mm in thickness), an electrolyte (0.1M lithium trifluoromethane sulfonimide (LiTFSI) in dimethoxyethane (DME)), the Celgard 2400 separator, and the as-prepared porous cathode. The cells were assembled in an Ar filled glove box with oxygen and water contents less than 1 ppm. They were gastight except for the cathode exposed to the DME-saturated O_2 atmosphere. The cell was operated under 1 atm of DME-saturated O_2 in a vessel.

For comparison, the cathodes with the commercial acetylene black carbon (AB) and the prepared GPPy as supports were prepared and assembled in the Li-O_2 cells as above.

1.3. Electrochemical measurements

The galvanostatic charge and discharge tests were conducted on a LAND CT2001A battery test system at current densities of 0.1 and 0.5 mA cm^{-2} with a lower voltage limit of 2.0 V (vs. Li/Li^+) and upper limit of 4.5V (vs. Li/Li^+) for GPPy and AB supported cells, or 4.0 V (vs. Li/Li^+) for TPPy supported cells at ambient temperature after a 6h rest period. All specific capacity results were calculated with the mass of the supports in air electrodes.

1.4. Characterization of air electrodes after discharge

Examination of a discharged electrode involved disassembling the cell in the glove box, rinsing the cathode three times with dimethyl carbonate, removing the solvent under vacuum, and then moving it into an airtight holder for the SEM test.

2 Lists of the figures

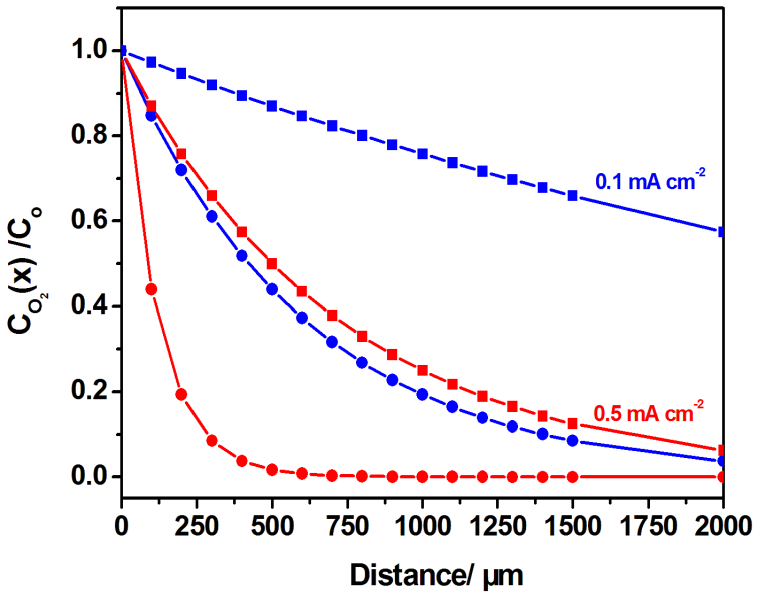

Fig. S1 Oxygen concentration along the 0.1 M Li^+ DME flooded porous electrode, the distance is the measure from the electrolyte–O_2 interface, $Co_2(x)$ is the concentration of O_2 in the electrolyte-filled pores at a distance x from the electrode–O_2 interface; Co is the O_2 solubility in the electrolyte.

The square and cycle symbols correspond to the air electrode at the onset of discharge and a discharge depth of 60% respectively. The calculated method is the same as in the reference [2].

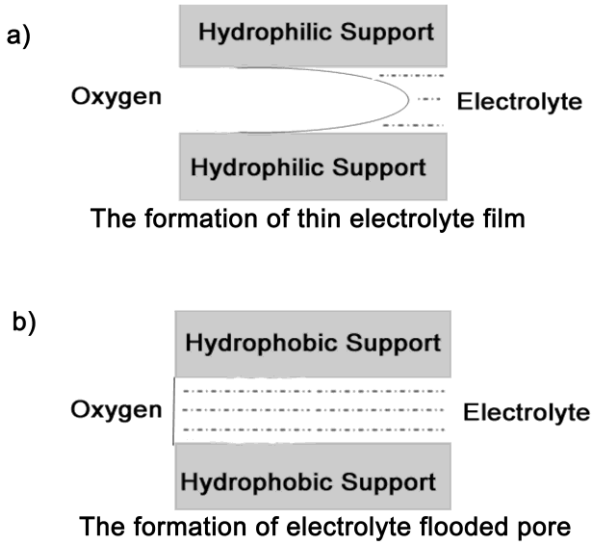

Fig. S2 Schematic views of a higher contact angle of electrolyte on a higher hydrophilic support (a) and a lower contact angle of electrolyte on a hydrophobic support (b).

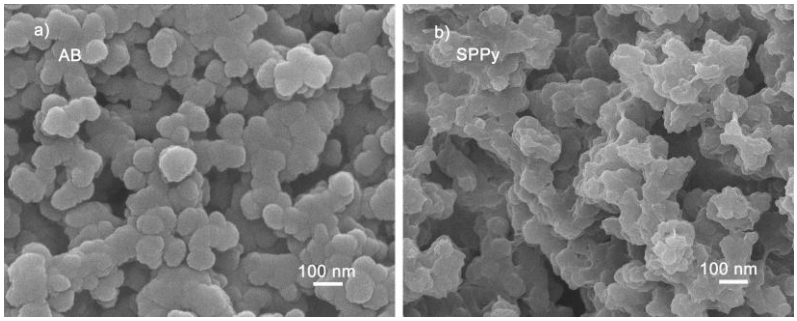

Fig. S3 SEM images of the commercial AB and prepared GPPy.

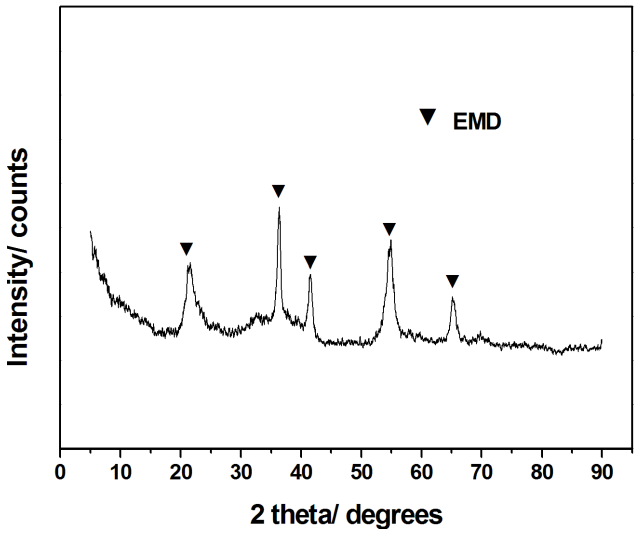

Fig. S4 XRD patterns of the employed EMD.

Table S1 BET results of the employed different supports.

	TPPy	GPPy	AB
BET surface area / m^2 g^{-1}	**25.04**	**42.06**	**65.29**
Pore Volume / m^3 g^{-1}	**0.035**	**0.075**	**0.111**

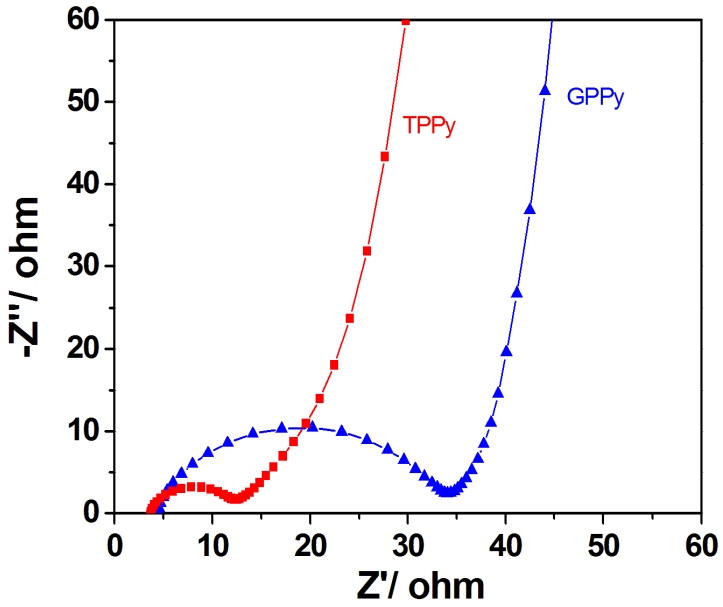

Fig. S5 AC impedance spectra before discharge of the Li-O_2 cells respectively based on GPPy and TPPy.

The discharge/charge performance of the TPPy based cell with only PPy and PVDF was also evaluated, as shown in Figure S6 (the blue one). The still very low charge voltage (from the initial to 700 mAh g^{-1} of charge) of the TPPy even without EMD demonstrates the good intrinsic performance of the TPPy. However, without EMD, the following charge voltage (after 700 mAh g^{-1} of charge) is increased, and the cell becomes less rechargeable than the EMD catalyzed one (only ~75% of the capacity was charged, charge capacity/ discharge capacity). Without the catalyst, the discharge capacity is also slightly decreased, probably owing to the effect of

hydrophilic property of the EMD in facilitating the formation of the three-phase-interface in the hydrophobic electrolyte. [3]

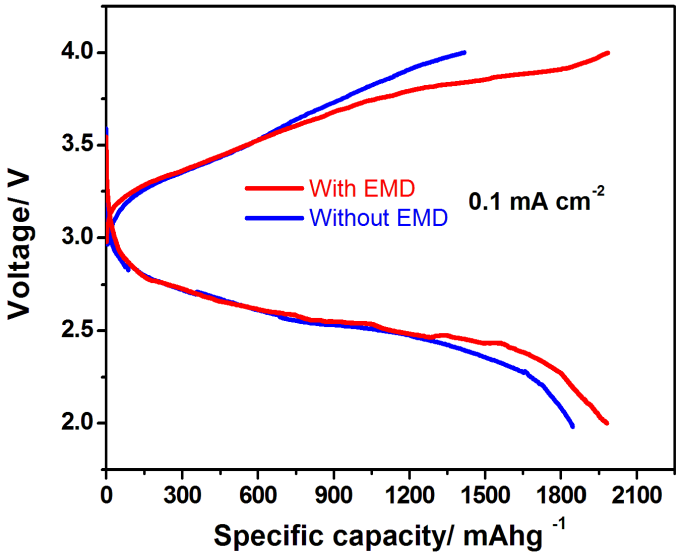

Fig. S6 The comparison of first discharge/charge profiles for the TPPy based Li-O_2 cells with and without EMD.

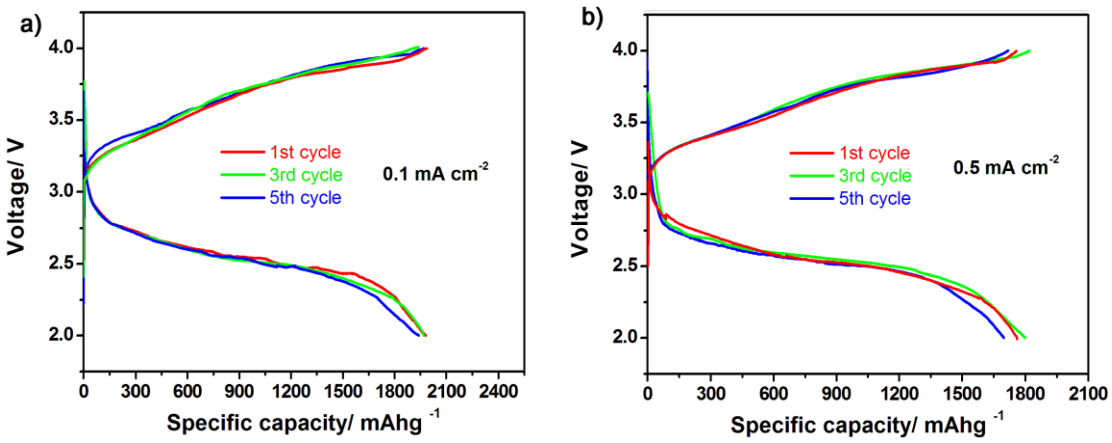

Fig. S7 Subsequent discharge/charge profiles of TPPy based Li-O_2 cell at 0.1 (a) and 0.5 mA cm^{-2} (b).

Table S2 Specific discharge capacities normalized with the total mass of the catalysts and

supports.

	Specific capacity/ mAh $g^{-1}_{support}$	Specific capacity/ mAh $g^{-1}_{support+catalyst}$
TPPy at 0.1 mA cm^{-2}	1982.02	726.74
TPPy at 0.5 mA cm^{-2}	1763.92	646.77
GPPy at 0.1 mA cm^{-2}	1302.66	477.64
GPPy at 0.5 mA cm^{-2}	928.50	340.45
AB at 0.1 mA cm^{-2}	967.97	354.92
AB at 0.5 mA cm^{-2}	358.01	131.27

The AB based electrode would bear high volume expansion after the discharge products deposition, demonstrated by many cracks in the electrode (Fig. S8), which leads to the loss of contact between electrode particles and the current collector. No similar results were observed in TPPy (Fig. 4c and d in the manuscript).

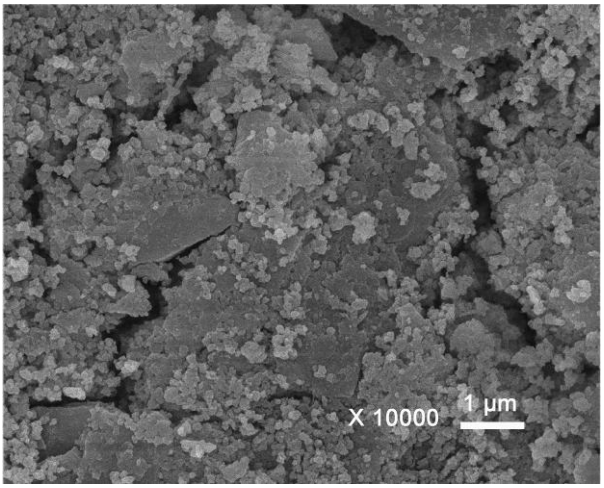

Fig. S8 SEM image of the fully discharged AB based electrode.

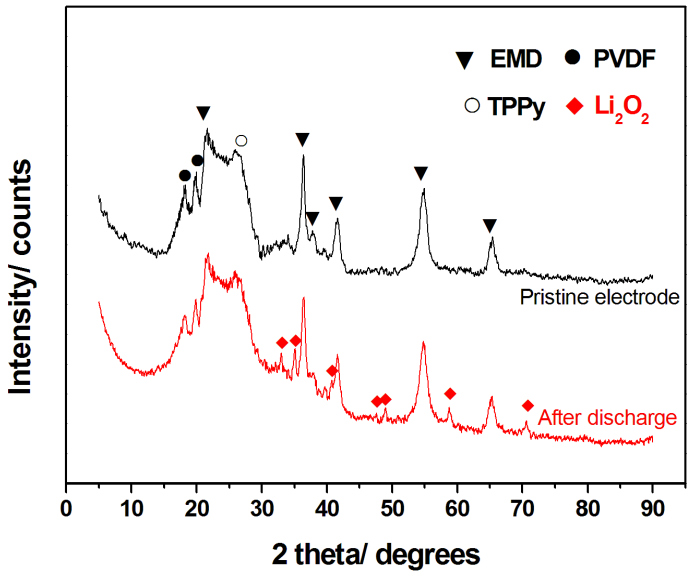

Fig. S9 XRD patterns of pristine and discharged TPPy based electrodes.

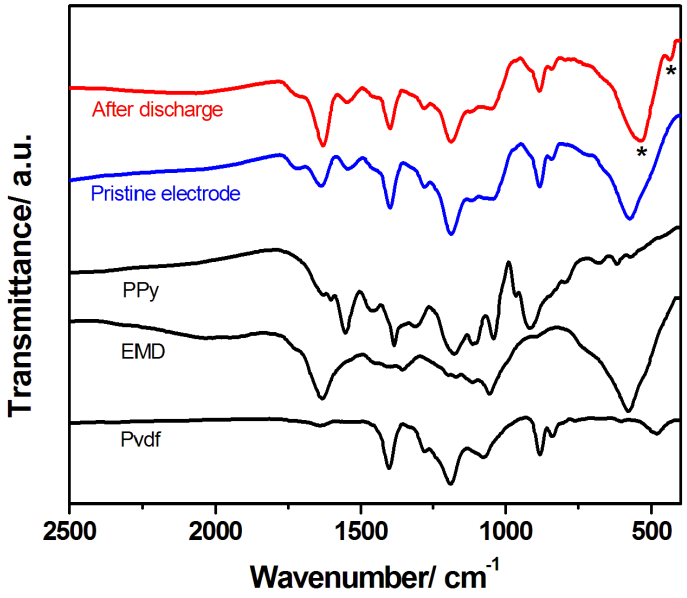

Fig. S10 FTIR spectra of the pristine and discharged electrodes.

As shown in the XRD patterns of the discharged electrode, Li_2O_2 is observed as the major discharge product in cathode (Fig. S9). Compared to the pristine electrode, the new absorbing peaks in the FTIR spectrum (Fig. S10) of the discharged electrode located at 400-500 cm^{-1} is mainly related to the formation of the Li_2O_2, whereas neither Li_2O, Li_2CO_3 nor other side products were detected. There is no obvious decomposition of the electrolyte, the PPy and PVDF detected.

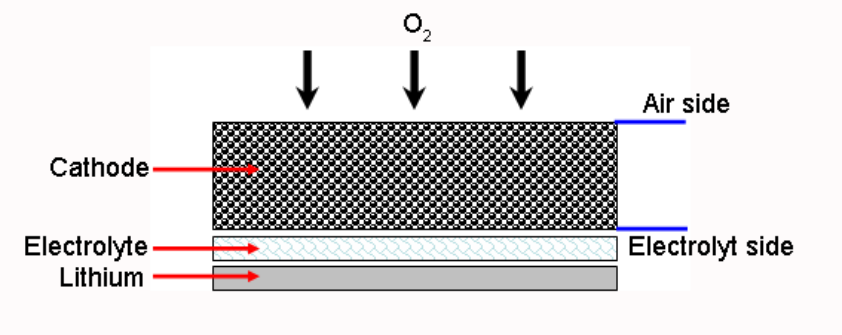

Fig. S11 Schematic images of the cell configuration.

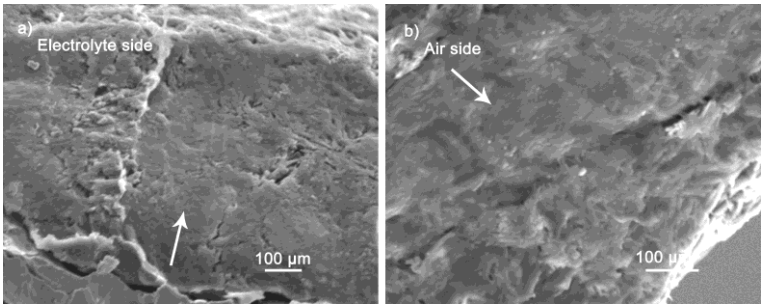

Fig. S12 Cross-sectional SEM images of the TPPy electrode at both electrolyte side and air side after full discharge. (The discharged product distribution is proportional to the oxygen concentration distribution)

The SEM images of both sides of the AB and GPPy electrodes after full discharge and charge were tested, as shown in Fig. S13 and Fig, S14, respectively.

It can be clearly observed that, at the air and electrolyte sides of the AB (Fig. S13) and GPPy based electrodes (Fig. S14), the morphologies of the discharge product distribution after discharge (Fig. S13a, b and Fig. S14a, b) and product decomposition after charge (Fig. S13c, d and Fig. S14c, d) are quite different from that in the TPPy electrode.

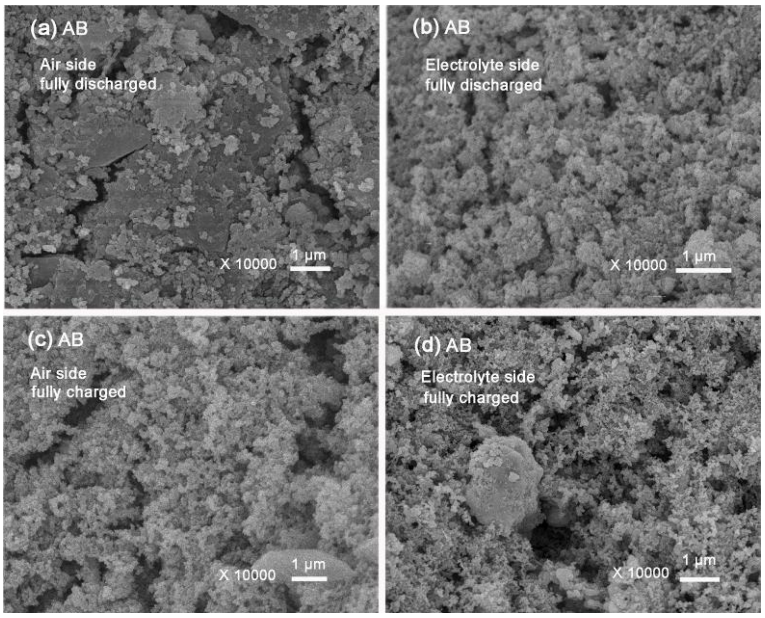

Fig. S13 SEM images of the AB based electrodes after full discharge at the air side (a) and at the electrolyte side (b); after full charge at the air side (c) and at the electrolyte side (d).

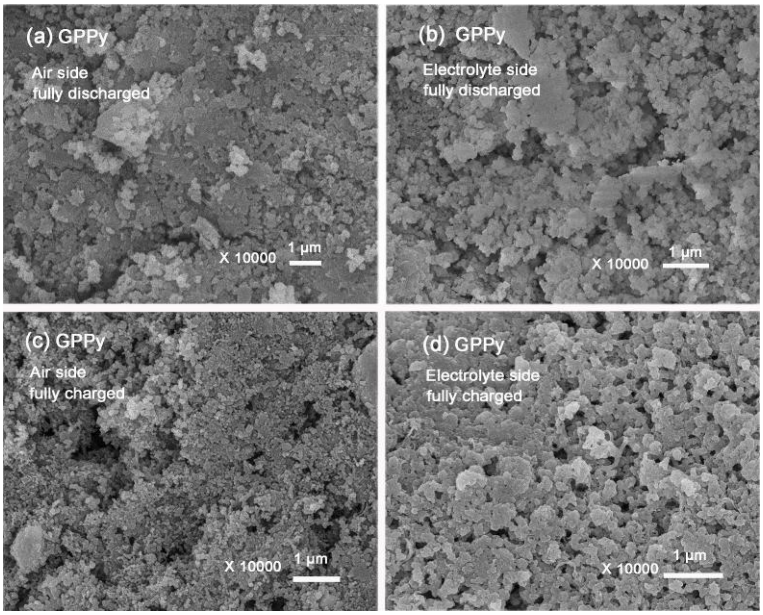

Fig. S14 SEM images of the GPPy based electrodes after full discharge at the air side (a) and at the electrolyte side (b); after full charge at the air side (c) and at the electrolyte side (d).

Unlike TPPy, the AB based electrode after full discharge demonstrates different morphologies at each sides (Fig. S13a and b): the air side is deposited with lots of the discharge products, and the nearly pitch-off of the electrode surface by the deposition of the discharge products can be observed (except for some cracks). However, because the similar outward of the discharge

products to the carbon particles, it may be difficult to distinguish them. While at the electrolyte side (Fig. S13b), the surface still shows lots of clear open pores with little morphology change in comparison with the pristine one, demonstrating little deposition of the discharge products. The air sides are deposited with more discharge products owing to its abound oxygen source; while the lower oxygen concentration at the electrolyte sides of AB electrode gives rise to less discharge products.

After the full charge (charging to 4.5V in this study), lots of the pores at air side of AB electrode are recovered (Fig. S13c). Because it is difficult to distinguish the discharge products from the carbon particles with the similar outwards, the SEM image here (Fig. S13c) could not directly demonstrate the amount of discharged product particles left or undecomposed after full charge. But the increase of the electrode particle size (about 130 nm) compared to the pristine AB (100 nm) demonstrates the existence of the uncharged precipitates at carbon particle surface. [2a] The accumulation of the undecomposed insulating products in the cathode during substantial discharge/charge process was known to lead to the high cell impedance and cycling capacity fade, which is consistent with our cycling results of AB shown in Fig. 3d.

Like the AB, the surface morphologies of the fully discharged GPPy based electrode at the air and electrode sides are also different (Fig. S14a and b). What different from the AB is the clearly observed deposition of the products at the electrolyte side of the GPPy electrode (Fig. S14b), demonstrated as the increase of the particle sizes and decrease of the porosity. [2a] The results could further prove the improved oxygen diffusion into the inner GPPy electrode over AB. The non-uniform distributions of the discharge products in both AB and GPPy electrodes are consistent with their lower discharge capacities than TPPy.

After charge, at the air side (Fig. S14c), the pores reappear at the surface of GPPy electrode, and the particle size in electrode increases much more slightly than that in AB electrode as compared to the pristine one, proving the improved decomposition of discharged products at the GPPy electrode air side during charge. At electrolyte side, a decrease of the discharged products is observed, but the particle size in electrode is still larger than that in the pristine, demonstrating the still existing uncharged products at the electrolyte side. The SEM results could prove the improved oxygen evolution and transfer in the GPPy electrode compared to AB, but it was still less effective than the TPPy.

3 Discussions

3.1 The improved oxygen diffusion by TPPy

Here we calculated the difference of the oxygen diffusion coefficients in the TPPy inner channels and the DME based electrolyte by Knudsen diffusion and molecular diffusion methods. The mean free path (λ) of O_2 molecule at 1.0 atm is ~130 nm, which is shorter than the TPPy inner pore's diameter (d) of 200 nm (0.1<d/λ<100), demonstrating the transfer resistance of the oxygen through the inner pore of TPPy would be the sum of the mass transfer resistance from the Knudsen diffusion resistance and molecular diffusion resistance, where the molecule diffusion resistance plays an essential role (the common pore-diameter at which the Knudsen Diffusion controlled the resistance for O_2 is ≤ 13 nm, λ/ d>10). According to the equation of the Knudsen diffusion coefficient:

$$D_{KA} = \frac{1}{3} \cdot \bar{v}_A \cdot r \quad \text{and} \quad \bar{v}_A = \left(\frac{8 \cdot R \cdot T}{\pi \cdot M_A}\right)^{1/2}$$

D_{KA} is the Knudsen diffusion coefficient; r diameter of the pore, m; $\bar{v}_A$ mean molecular velocity, m s^{-1}; R molar gas constant, 8.314 J mol^{-1}; T thermodynamic temperature, K; M_A molecular weight, Kg mol^{-1}.

$$D_{KA} = \frac{1}{3} \cdot \left(\frac{8 \cdot R \cdot T}{\pi \cdot M_A}\right)^{1/2} \cdot r$$

$$= \frac{1}{3} \times \left(\frac{8 \times 8.314 \times 298 \ \text{J mol}^{-1}}{3.14 \times 32 \times 10^{-3} \ \text{Kg} \ \text{mol}^{-1}}\right)^{1/2} \times 200 \times 10^{-9} \ \text{m} = 2.96 \times 10^{-5} \ \text{m}^2/\text{s},$$

even with the modification of porosity (ε , ~0.64, inner pore volume/total volume= (100×100)/(125×125)) and tortuosity (σ , ~ 1, as shown in the TEM image (Fig. 2b) of the TPPy with vertical pipeline), the D_{KA} is still in the order of 10^{-5}.

Because there exists little bending in the TPPy (shown in both TEM (Fig. 2b) and SEM (Fig.2a)), and the diffusion distance in hollow channel of the TPPy is almost equal to the real straight-line length, the tortuosity σ would be close to 1.

The tortuosity of the TPPy channel is approximately described by the SEM image. [4] We choose the special case with bentest morphology shown in the SEM image (inset of Fig. 2a), and the tortuosity σ would be:

$$\sigma = \frac{\text{Length of the curve between two points (s)}}{\text{Straight - line distance between two points (L)}} = 1.2$$

So, the tortuosity σ would be smaller than 1.2.

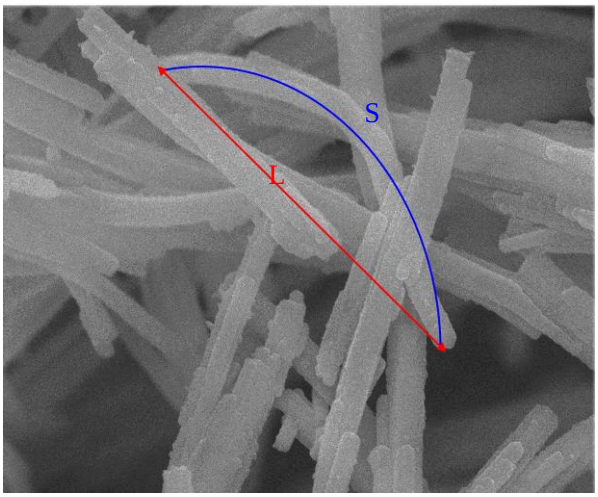

Inset of Fig. 2a. The SEM image of the TPPy.

$D_{KE} = \frac{\varepsilon}{\sigma} \cdot D_{KA}$ = 1.89 $\times 10^{-5}$ m^2/s (ε =0.64 and σ =1) as the effective Knudsen diffusion coefficient, where ε is the porosity of the electrode, and σ is the tortuosity. Even if the inner surface of the electrode would be suspended with some liquid and the inner vacant diameter is smaller than 200 nm, the D_{KA} is still in the range of 10^{-5} -10^{-7} orders of magnitude.

The final effective diffusion coefficient in hollow TPPy follows the equation of

$$\frac{1}{D_E} = \frac{1}{D_{KE}} + \frac{1}{D_{KA}}$$

D_{KA} is the molecular transfer coefficient of O_2, which is ~ 2.3×10^{-5} m^2/s at room temperature and 1atm. So, D_E = 0.96 $\times 10^{-5}$ m^2/s.

The diffusion coefficient of O_2 in the electrolyte DME is about 4×10^{-5} cm^2/s (4×10^{-9} m^2/s) [2a]. Compared with the resistance of the O_2 transferring in the liquid electrolyte, the O_2 transfer in the TPPy inner pores could be much faster and easier (with significantly improved diffusion coefficient). The oxygen would prefer to transfer through the inner channel of TPPy. It is noticeable that the above calculation of the diffusion coefficient through the hollow TPPy is based on the premise that the electrolyte would not go into the inner pores.

The new calculated oxygen concentration distribution along the electrode thickness with the effective diffusion coefficient of 0.96 $\times 10^{-5}$ m^2/s is shown as Fig. S15. It obviously demonstrates the improved oxygen diffusion and higher uniform oxygen distribution by TPPy, which is in good agreement with Fig. 1b and the high uniform distribution of the discharge products as shown in Fig. S12.

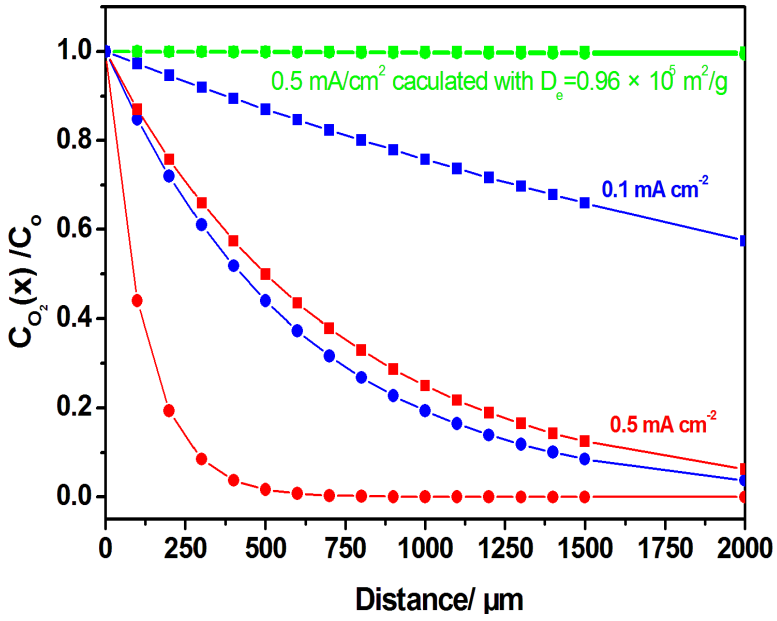

Figure S15 The oxygen gradients cross the flooded porous cathode (red and green) and with favorable effect of the TPPy (blue). The square and cycle symbols correspond to the air electrode at the onset of discharge and a discharge depth of 60% respectively. The calculated method is the same as in the reference

3.2 The improved three-phase-interface in TPPy

In order to further demonstrate the O_2 and liquid electrolyte volume occupation and prove the increased three-phase interface in the TPPy based electrode, the electrolyte volume occupation of the porous electrode was obtained by a calculation from discharged products and the electrolyte uptaking measurement.

3.2.1 Calculation

As seen in Fig. S12, the distribution of the discharge products in air electrode is very uniform with high packing density, indicating the uniform liquid electrolyte containing reaction space in the electrode. We tried to calculate the occupation volume ratio of the discharge products in the

discharged electrode to quantitatively evaluate the volume occupation of the electrolyte in the electrode.[5] The calculation is as follows:

The pristine TPPy electrode porosity is ~0.85 (by Archimedes method), and the carbon or TPPy loadings in electrodes were ~ 65 mg $_{PPy}$ and 59 mg $_{carbon}$ per cm^2 electrode. The mass density and molecule weight of Li_2O_2 are 2.14 g/cm^3 and 45.88 g/mol, respectively. So the theoretical specific capacity of the TPPy electrode on account of all the volume is occupied by the discharge products could be

$$\frac{0.15cm \times 1cm^2 \times 0.85 \times 2.14g/cm^3 \times 96500c/mol}{45.88g/mol \times 3600s/h \times 65mg/1000} = 2.450 \text{ Ah/g} = 2450 \text{ mAh/g}$$

At 0.5 mA/cm^2, the discharge capacity of the TPPy based electrode is about 1800 mAh/g, which corresponds to the blockage of the electrode porosity of 0.62 ($\frac{1800 \times 0.85}{2450}$) of and 0.23 (0.85-0.62) left (without consideration of the side reaction which would influence the capacity). Because of the highly uniform oxygen distribution and furthermore, considering the origin of O_2 and electrolyte to the discharge products, the volume ratio of 0.62 occupied by the discharge products is reasonably derived from the similar amount of volume occupation of electrolyte in the electrode. In other words, the volume occupation of the electrolyte in the electrode could be about 0.62 (confirmed by the electrolyte uptake measurement shown below). The left volume ratio of the 0.23 could be related to the volume of the electrode with filled gas but without permeated electrolyte (If at 0.1 mA cm^{-2}, the value would be 0.12, which might be more accurate). Furthermore, as observed from the cross-section SEM images that there was almost no apparent vacant space left in the fully discharged electrode (Fig, S12), most of the left ratio could correspond to the volume from the kept-open inner pores of the TPPy, which kept electrolyte-free and without deposition of the products at the end of the discharge (insets of Fig. 4c,d).

3.2.2 Electrolyte uptake measurement

We carried out the tests of the electrolyte uptake for TPPy and AB based electrodes, respectively. After soaked in the electrolyte (0.1M Li^+ in DME) for 1h, the electrodes were taken out for measurements by a modified Archimedes method at room temperature and 101.325 KPa. The AB based electrode (14 mm in diameter, 1.5 mm in thickness of the electrode, 0.23 cm^3, and 80% total porosity) demonstrates electrolyte uptake of about 0.18 mL, which corresponds to ~78

% of the electrode volume (~97% of the total porosity), and the uptake amount by TPPy based electrode (85% porosity) is 0.144 mL, ~62.6 % of the electrode (~73.6 % of the total porosity), which is quite consistent with the value obtained from the calculated volume ratio of discharged products. Because of the small liquid electrolyte uptake amount and the high volatility of the DME (saturated vapor pressure of DME is as high as 538 KPa at 293K), the volume value might be not precise enough, but clearly demonstrating the effectiveness of the TPPy.

The TPPy based electrode demonstrates less organic electrolyte uptake, more gas diffusion channels and larger three-phase-interface.

Reference

1 a)J. Read, *J. Electrochem. Soc.*, 2002, **149**, A1190.; b) M. Mirzaeian, P.J. Hall, *J. Power Sources*, 2010, **195**, 6817.

2 a)Y.-C. Lu, D. G. Kwabi, K. P. C. Yao, J. R. Harding, J. Zhou, L. Zuin, Y. Shao-Horn, *Energy Environ. Sci.*, 2011, **4**, 2999.; b) J. Read, K. Mutolo, M.Ervin, W. Behl, J. Wolfenstine, A. Driedger, D. Foster, *J. Electrochem. Soc.*, 2003, **150**, A1351.; c) I. Kowalczk, J. Read, M. Salomon, *Pure Appl. Chem.*, 2007, **79**, 851.

3 Y. Cui, Z. Wen, S. Sun, Y. Lu, J. Jin, *Solid State Ion.*, 2012, **doi:10.1016/j.ssi.2012.01.021**

4 W. Zhou，R. Xiang, F. Wei, G. Luo, *Journal of Chinese Electron Microscopy Society*, 2006, **25**, 125-129.

5 Z.P. Zheng, R.Y. Liang, M. Hendrickson, E.J. Plichta, *J. Electrochem. Soc*., 2008, **155**, A432-A437.